THE JOURNAL OF BIOLOGICAL CHEMISTRY VOL. 286, NO. 31, pp. 27528–27536, August 5, 2011


# Interaction of Actin with Carcinoembryonic Antigen-related Cell Adhesion Molecule 1 (CEACAM1) Receptor in Liposomes Is $Ca^{2+}$- and Phospholipid-dependent*[S]

Received for publication, March 2, 2011, and in revised form, June 7, 2011 Published, JBC Papers in Press, June 13, 2011, DOI 10.1074/jbc.M111.235762

**Rongze Lu**[‡1], **Michiel J. M. Niesen**[§1], **Weidong Hu**[§1], **Nagarajan Vaidehi**[§], **and John E. Shively**[§2]

*From the* [‡]*Irell and Manella Graduate School of Biological Sciences and the* [§]*Department of Immunology, Beckman Research Institute of City of Hope, Duarte, California 91010*

**The regulation of binding of G-actin to cytoplasmic domains of cell surface receptors is a common mechanism to control diverse biological processes. To model the regulation of G-actin binding to a cell surface receptor we used the cell-cell adhesion molecule carcinoembryonic antigen-related cell adhesion molecule 1 (CEACAM1-S) in which G-actin binds to its short cytoplasmic domain (12 amino acids; Chen, C. J., Kirshner, J., Sherman, M. A., Hu, W., Nguyen, T., and Shively, J. E. (2007) *J. Biol. Chem.* 282, 5749–5760). A liposome model system demonstrates that G-actin binds to the cytosolic domain peptide of CEACAM1-S in the presence of negatively charged palmitoyl-oleoyl phosphatidylserine (POPS) liposomes and $Ca^{2+}$. In contrast, no binding of G-actin was observed in palmitoyl-oleoyl phosphatidylcholine (POPC) liposomes or when a key residue in the peptide, Phe-454, is replaced with Ala. Molecular Dynamics simulations on CEACAM1-S in an asymmetric phospholipid bilayer show migration of $Ca^{2+}$ ions to the lipid leaflet containing POPS and reveal two conformations for Phe-454 explaining the reversible availability of this residue for G-actin binding. NMR transverse relaxation optimized spectroscopic analysis of $^{13}C$-labeled Phe-454 CEACAM1-S peptide in liposomes plus actin further confirmed the existence of two peptide conformers and the $Ca^{2+}$ dependence of actin binding. These findings explain how a receptor with a short cytoplasmic domain can recruit a cytosolic protein in a phospholipid and $Ca^{2+}$-specific manner. In addition, this model system provides a powerful approach that can be applied to study other membrane protein interactions with their cytosolic targets.**

Monomeric G-actin is recruited to the plasma membrane in response to a variety of cell receptor activation signals (1–4). Although much is known about subsequent steps, including actin polymerization, branching, and participation in functions such as cell motility, less is known about the regulation of the initial G-actin recruitment event. Among the many cell surface receptors that bind G-actin when activated, the so-called "short form" of CEACAM1[3] stands out as a rather simple example in that it is a single-pass transmembrane protein with a cytoplasmic domain of only 12 amino acids. When a single amino acid phenylalanine 454 in the cytoplasmic domain is mutated to alanine (F454A), it no longer binds G-actin in *in vitro* assays, and when transfected into MCF7 cells that form a lumen with wild-type CEACAM1-S, it no longer forms a lumen in three-dimensional culture (5). Intrigued by the ability of such a short stretch of amino acids to convey G-actin binding in response to the homotypic cell-cell interaction function of CEACAM1, we speculated that the adjacent membrane environment and $Ca^{2+}$ signaling may play a role in regulating the binding, otherwise binding would be constitutive and irreversible. Given the close proximity of the cytoplasmic domain of CEACAM1 to the lipid bilayer and the inherent asymmetry of the lipid bilayer with respect to charge, we propose that negatively charged phospholipids would attract $Ca^{2+}$ in response to cell-cell interactions because $Ca^{2+}$ signaling almost always accompanies cell-cell interactions (6, 7). Furthermore, $Ca^{2+}$ recruited to the negatively charged inner leaflet of the plasma membrane would effectively promote the interaction of the cytoplasmic domain of CEACAM1 with G-actin. To test this hypothesis, we generated an *in vitro* model of the peptide-actin interaction in the context of negatively charged liposomes in the presence or absence of $Ca^{2+}$ and analyzed their interactions by a combination of fluorescent bead analysis, NMR TROSY experiment, molecular dynamics (MD) simulation, and surface plasmon resonance analysis.

## EXPERIMENTAL PROCEDURES

*Preparation of Liposome-coated Glass Beads*—Palmitoyl-oleoyl phosphatidylserine (POPS) and palmitoyl-oleoyl phosphatidylcholine (POPC) powders (Avanti Polar Lipids) were stored in chloroform at 25 mg/ml. Five $\mu$l of stock phospholipid solution in a glass tube was vaporized under argon gas to from a thin and even membrane on the glass tube. Phospholipid was dissolved in 100 $\mu$l of PBS, vortexed, and subjected to extrusion through a 200-nm membrane 11–13 times (Avanti Polar Lipids).

* This work was supported, in whole or in part, by National Institutes of Health Grant CA 84202.

[S] The on-line version of this article (available at http://www.jbc.org) contains supplemental Tables S1 and S2, Figs. S1–S6, and an NMR Discussion.

[1] These authors contributed equally to this work.

[2] To whom correspondence should be addressed: Dept. of Immunology, Beckman Research Institute of City of Hope, 1450 East Duarte Rd., Duarte, CA 91010. Tel.: 626-359-8111 (ext. 62601); E-mail: jshively@coh.org.

[3] The abbreviations used are: CEACAM1, carcinoembryonic antigen-related cell adhesion molecule1; CEACAM1-S, short isoform of CEACAM1; MD, molecular dynamics; MUA, mercaptoundecanoic acid; POPC, palmitoyl-oleoyl-phosphatidylcholine; POPS, palmitoyl-oleoyl-phosphatidylserine; TROSY, transverse relaxation optimized spectroscopy.

Glass microspheres (4.5 $\mu$m; Bangs Laboratories, Inc.) were cleaned in "piranha solution" (30% $H_2O_2$ and concentrated $H_2SO_4$ 1/4 (v/v) for 3 min at 80 °C, use extreme caution!) followed by extensive washing with water on a clean sintered glass funnel. Clean glass beads were diluted in water ($10^8$ beads/$\mu$l) and stored at 4 °C. One to 2 $\mu$l of suspended glass beads were incubated with 100 $\mu$l of liposome at 37 °C for 2 h. Liposome-coated glass beads were centrifuged at 4000 rpm for 1 min and washed three times with PBS to remove unbound phospholipid. Glass bead-supported phospholipid membranes were incubated with MUA (mercaptoundecanoic acid)-CEACAM1-S peptide (0.2 mg/ml) for 1 h at 37 °C and collected by centrifugation. Peptide-liposome-coated glass beads further incubated with 1% BSA in PBS for 1 h and washed three times using 1% BSA/PBS. G-actin (100 $\mu$g/ml) or rhodamine-actin (100 $\mu$g/ml) in the presence or absence of 1 mM $CaCl_2$ was incubated with glass beads for 1 h. In the last step, FITC-conjugated anti-actin antibody was incubated with glass beads. Flow cytometry was used to detect the florescence of rhodamine-actin or FITC-conjugated anti-actin antibody on a BD FACS caliber. Single beads were selected for analysis based on forward and side scatter analysis (>80%).

*Surface Plasmon Resonance Assay*—Surface plasmon resonance assays were performed on a Biacore T100 (BIAcoreAB) instrument. Liposome or liposome-containing CEACAM1-S MUA-peptide was prepared using the same method as above. The HPA sensor chip (GE Healthcare) was washed with 40 mM $\beta$-octylglucoside at a flow rate of 5 $\mu$l/min for 5 min. Liposomes composed of POPS (2 mg/ml) containing CEACAM1-S MUA-peptide (0.2 mg/ml) in PBS were injected at flow rate of 1 $\mu$l/min. Unbound lipid was washed by increasing the flow rate. One percent BSA in PBS was injected to block the sensor chip surface. Actin (0.2 mg/ml) was injected plus or minus 1 mM $CaCl_2$ at a flow rate of 20 $\mu$l/min. 0.5 M EDTA (10 $\mu$l) was used to regenerate the HPA sensor chip surface. Liposomes without CEACAM1-S MUA-peptide were immobilized to HPA sensor chip and used as a blank.

*MD System Preparation*—A molecular model of the transmembrane and cytoplasmic domain of CEACAM1-S derived previously using homology modeling methods was used in this study (5). The F454A mutant peptide was generated by using the side chain coordinates of the $C_\beta$ of Ala-454 in place of Phe-454. The CEACAM1-S peptide was placed in a simulation box with preequilibrated POPS lipids (courtesy of Peter Tieleman). The center of the peptide and the lipid bilayer were aligned, and the peptide was oriented with its first principal axis perpendicular to the lipid bilayer. To create five different starting conformations the peptide was rotated around its first principal axis by 0, 45, 90, 180, and 270°, respectively.

To pack the lipid around the peptide we used the *inflategro* package in GROMACS (8). First, the lipid bilayer was expanded by a factor of 4, and lipid molecules within 14 Å of the peptide were removed to avoid clashes between lipid and peptide atoms. To generate an asymmetric lipid bilayer, the POPS lipids of the outer leaflet and 50% of the POPS in the inner leaflet were converted into POPC. Lipids were iteratively packed around the CEACAM1-S peptide by shrinking the bilayer area by 5% using the *inflategro* package in GROMACS, with steepest descent energy minimization, using position restraints to prevent the peptide from moving, performed after every iteration. This procedure was repeated until an area per lipid close to the experimental value of 65.8 $A^2$ (9) was reached.

Single-point charge water molecules (10) were added on both sides of the lipid bilayer, and an appropriate number of sodium ions were added in the water to neutralize the system. For each of the five conformations we also generated a system with 2 additional $Ca^{2+}$ ions that were neutralized by 4 $Cl^-$ ions. All ions were added by displacing random water molecules using the *genion* command in GROMACS. The final systems were minimized by steepest descent energy minimization with a maximum force of 1000 kJ/mol per nm as convergence criterion.

*MD Simulation Parameters*—MD simulations on CEACAM1-S in a lipid bilayer consisting of POPS and POPC were performed using GROMACS 4.0.5 (11) and the GROMOS96 53a6 forcefield (12) extended with Berger lipid parameters (13). Short range nonbonded interactions were truncated at 1.2 nm, with the neighbor list updated every 10 fs. To account for the cutoff in the van der Waals interactions, long range dispersion correction was applied to energy and pressure terms. Long range electrostatics were calculated using the smooth particle mesh Ewald method (14). Bonds were constrained using the LINCS algorithm (15) to allow for a time step of 2 fs. For continuity, periodic boundary conditions were applied in every dimension.

MD simulations were performed on five starting conformations of CEACAM1-S in lipid without $Ca^{2+}$ ions and five conformations of CEACAM1-S in lipid with $Ca^{2+}$ ions. Each system was equilibrated by performing 100 ps of MD at 310 K using a NVT ensemble followed by 5 ns of MD under NPT conditions with a pressure of 1 bar. The velocity-rescaling thermostat (16) was used for temperature coupling during the equilibration and a Parrinello-Rahman barostat (17, 18) for pressure coupling. The CEACAM1 peptide was kept in place during these equilibration steps using position restraints of 1000 kJ/mol per $nm^2$.

After the systems were equilibrated at the correct temperature and pressure, MD simulations of 100 ns were performed for each of the 10 conformations, using a NVT ensemble with a Nosé-Hoover thermostat (19). Simulations on the F454A mutant were performed over 40–100 ns for a total of ~600 ns. Data were not collected for the first 5 ns of each simulation.

*K-Means Clustering Analysis*—The interatomic distances between the $C_\alpha$, $C_\beta$, and $C_\gamma$ atoms of the CEACAM1-S peptide were extracted every 10 ps from the MD trajectories. The first 5 ns of each trajectory was left out to avoid not well equilibrated conformations. The distances of all simulations were combined into one distance matrix for clustering analysis, leading to a total of 9510 sampled conformations with each conformation expressed as 4950 interatomic distances. The distance matrix was grouped into two clusters using a K-Means clustering algorithm. The process was repeated 10 times to verify that the clusters were reproducible; grouping into three clusters was attempted but was not reproducible.

*Preparation of Samples for NMR*—Fmoc (*N*-(9-fluorenyl)-methoxycarbonyl)-Phe-OH-$^{13}C_9$, $^{15}N$ 98 atom % $^{13}C$, 98 atom

% $^{15}N$ was purchased from ISOTEC. C18 Sep-Pak cartridges were purchased from Waters (Ireland). POPS (porcine brain) and POPC (chicken egg) were purchased from Avanti Polar Lipids. Nonmuscle actin (99% pure) was purchased from Cytoskeleton.

To remove the residual TFA from the synthesized peptide, a C18 cartridge was conditioned using 70% acetonitrile solution followed by 1% acetic acid wash. After the peptide solution was loaded onto the cartridge, the column was washed using 1% acetic acid, then eluted with 70% acetonitrile-water. Samples were lyophilized and stored at −80 °C. The peptide concentration was determined using an NMR method (20). Bulk solutions of POPS and POPC were prepared by dissolving 100 mg of each lipid in 4 ml of chloroform, flushed with argon, and stored at −20 °C.

For POPS or POPC liposomes, 288 or 268 μl of bulk solution was transferred to a 1.5-ml polypropylene tube, and the solvent was evaporated under argon and further dried overnight under vacuum. To the dry lipid film, 400 μl of 50 mM phosphate buffer (90% $D_2O$, pH 7.0) and 1.5 μl of 166 mM EDTA solution were added, vortexed, and sonicated for 30 min or until the lipid solution became transparent. The 400-μl liposome solution was then mixed with 100 μl of 0.5 mM MUA-$^{13}C$, $^{15}N$-Phe-CEACAM1-S peptide in 50 mM phosphate buffer (90% $D_2O$, pH 7.0), and 1 mM tris (2-carboxyethyl)phosphine. The sample was then transferred to the NMR tube and flushed with argon gas. For the study of the complex with actin, 460 μl of the MUA-CEACAM1-S peptide-liposome solution was added to 2 mg of actin powder. After vigorous vortexing, the solution was transferred to an argon-flushed Shigemi NMR tube. For the sample in the presence of $Ca^{2+}$, the $Ca^{2+}$ was added after the addition of actin at a final $Ca^{2+}$ concentration of 5 mM. For the mixed POPS/POPC liposome system, 144 μl of POPS and 134 μl of POPC were taken from the bulk POPS and POPC solution, respectively, and the two lipids were mixed well before evaporating the solvent.

*NMR Experiments*—We used $^{13}C$-labeled Phe in the CEACAM1-S peptide as a probe because the chemical shifts of the aromatic ring are well separated from signals of the lipid. Because the CEACAM1-S peptide is inserted into the liposome through the MUA-aliphatic group, there is significant line broadening of the NMR signal from $^{13}C$-labeled Phe aromatic ring. For 0.1 mM concentration of peptide, the peptide signal is very weak from constant-time $^{13}C$-$^{1}H$ heteronuclear single-quantum coherence experiment (21). Much better signal intensity (>2-fold) was obtained from the aromatic ring using constant time TROSY experiment (22). The experiments were carried out at 35 °C on a 600-MHz Bruker instrument equipped with a cryoprobe. The constant time duration, spectrum width, and total number of free induction decays for the $^{13}C$ dimension are 17.6 ms, 4 ppm, and 20, respectively. For the $^{1}H$ dimension, the total number of points and spectrum width are 2048 and 14 ppm, respectively. The recycle delay is 1.2 s. The experimental time is about 18 h with the number of scans ranging from 2200 to 2560. The TROSY data were processed using the NMRPipe software (23) and analyzed using the NMRView program (24).

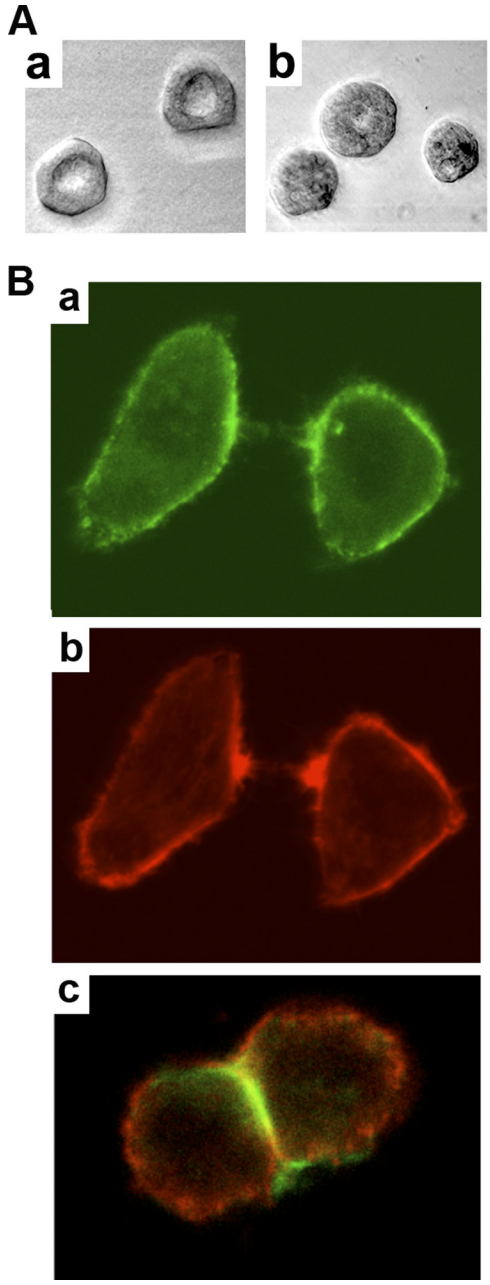


FIGURE 1. **CEACAM1-S induces lumen formation and migrates to cell-cell contacts.** *A*, expression of wild-type CEACAM1-S induces 97% lumen formation in transfected MCF7 cells grown in three-dimensional culture (300 acini counted; representative acini shown in *a*), whereas the cytoplasmic domain mutant F454A suppressed lumen formation by >90% (16% lumen formation, 300 acini counted; representative acini shown in *b*). The data are taken from Chen *et al.* (5) with permission. *B*, HeLa cells transfected with a CEACAM1-S-GFP fusion protein (5) showing accumulation of CEACAM1-S (*green*, *a*) and F-actin (*red*, *b*) at the cell surface of single cells making initial cell-cell contacts with almost complete redistribution of their CEACAM1-S between the cells (*c*) when cell-cell contact is complete.

## RESULTS

*Lipid Bilayer Model System*—CEACAM1 has two cytoplasmic domain isoforms, of which the short isoform (CEACAM1-S) is sufficient to induce lumen formation when expressed in the breast cancer cell line MCF7 and grown in three-dimensional culture (Fig. 1*A*). When CEACAM1-S is expressed in cells that undergo cell-cell contact, CEACAM1-S

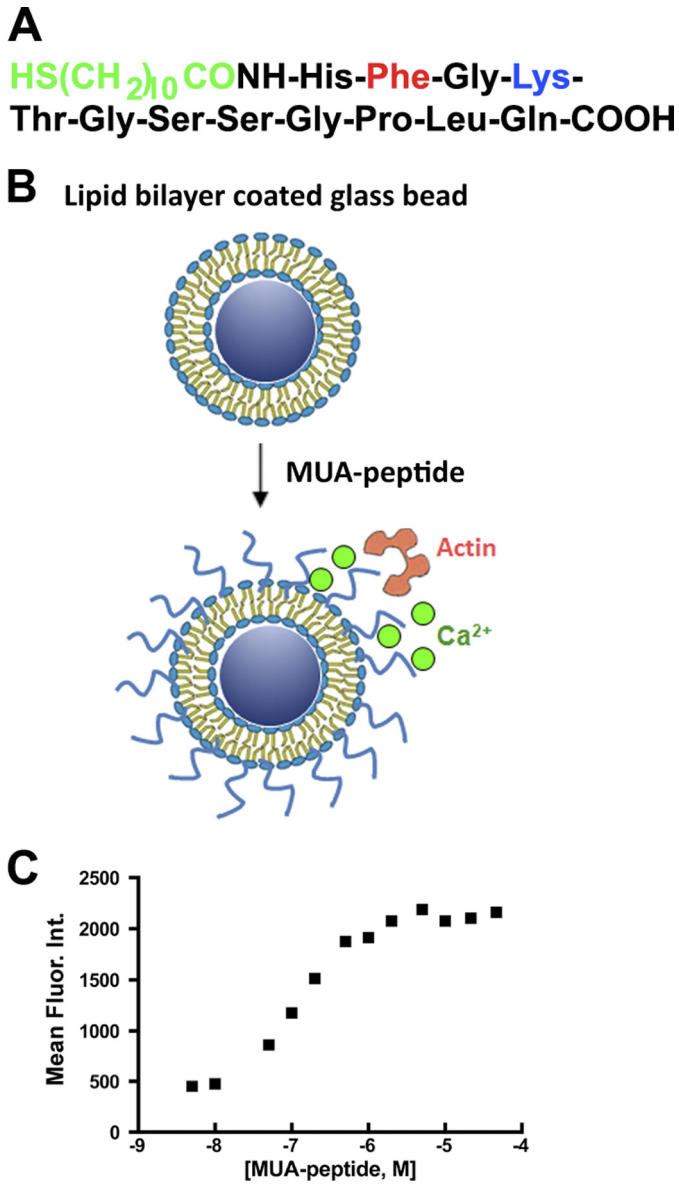


FIGURE 2. **Generation of lipid-embedded cytoplasmic domain of CEACAM1-S.** The cytoplasmic domain of CEACAM1-S has 12 amino acids that when synthesized with an *N*-acyl-MUA (*A*) spontaneously inserts into 4.5-$\mu$m glass beads coated with POPS or POPC liposomes used in actin binding experiments (*B*) and can be quantitated with fluorescent-tagged anti-peptide antibodies (mean fluorescence intensity *versus* concentration of peptide, *C*).

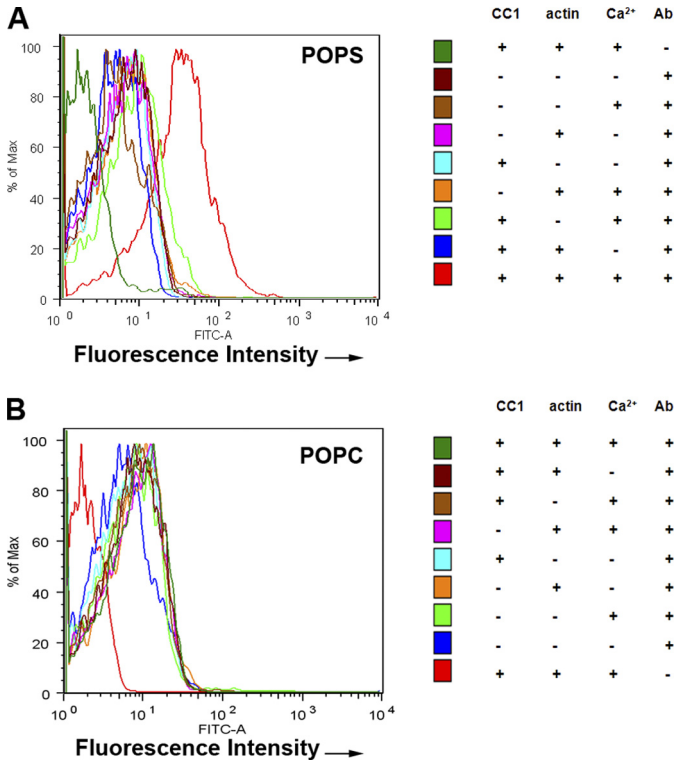


FIGURE 3. **G-actin binds to CEACAM1-S peptide in POPS liposome coated glass beads in a $Ca^{2+}$-specific manner.** *A*, POPS liposome-coated 4.5-$\mu$m glass beads ± *N*-acyl-MUA-wild-type peptide ± rhodamine G-actin (or ± G-actin and ± anti-G-actin antibody) ± 1 mM $Ca^{2+}$ in PBS plus 1% BSA were analyzed by FACS (see *right panel* for details). Significant actin binding is only seen for the fully reconstituted system. *B*, same experiment as in *A* except POPC liposome-coated glass beads were used. There was no significant actin binding even for the fully reconstituted system.

migrates to the cell-cell contact region along with F-actin (Fig. 1*B*). Although we have shown that the initial interaction of the short cytoplasmic domain is with G-actin (5), the small size of this domain and its close proximity to the inner leaflet of the plasma membrane prompted us to investigate the role of the microenvironment in its interaction with G-actin in a model system. The model comprises a phospholipid bilayer coated onto 4.5-$\mu$m glass beads into which is inserted an MUA version of the 12-amino cytoplasmic domain of CEACAM1-S (Fig. 2, *A* and *B*). The MUA-peptide spontaneously inserts into the lipid bilayer in a saturable manner that can be quantitated by fluorescently tagged anti-peptide antibodies using flow cytomtery (Fig. 2*C*). The liposome-glass bead displayed peptide is then incubated with either G-actin (detected by anti-actin antibody plus fluorescent-tagged secondary antibody) or rhodamine-actin in the presence or absence of $Ca^{2+}$. Two phospholipid environments were analyzed: POPS, an abundant negatively charged phospholipid on the inner leaflet of the plasma membrane, and POPC, the most abundant neutral phospholipid on the outer leaflet. As shown on Fig. 3*A*, G-actin binds to the peptide only in POPS with $Ca^{2+}$, but not in POPC with or without $Ca^{2+}$ (Fig. 3*B*). To test the validity of this model system further, we repeated the experiment with two mutated versions of the peptide, the F454A mutation, which abrogates *in vitro* binding to G-actin and *in vivo* lumen formation, and the K456A mutation, which enhances G-actin binding (5). Consistent with the previous studies, the F454A mutation abrogated actin binding (Fig. 4*A*), and the K456A mutation enhanced actin binding (Fig. 4*B*). These results not only confirm our previous findings but also suggest that both the lipid and $Ca^{2+}$ environment enable the interaction, thus providing a context for the regulation of the interaction. They also show that these liposomes can be used to query the interaction of a transmembrane protein interacting with intracellular proteins.

*MD Simulations*—To investigate any direct effect $Ca^{2+}$ ions may have on the conformation of the CEACAM1-S peptide in its native lipid environment we performed a total of 1 $\mu$s of MD simulations on CEACAM1-S embedded in an asymmetric lipid bilayer. To reduce bias caused by the choice of an initial conformation we have initiated simulations from five unique start-

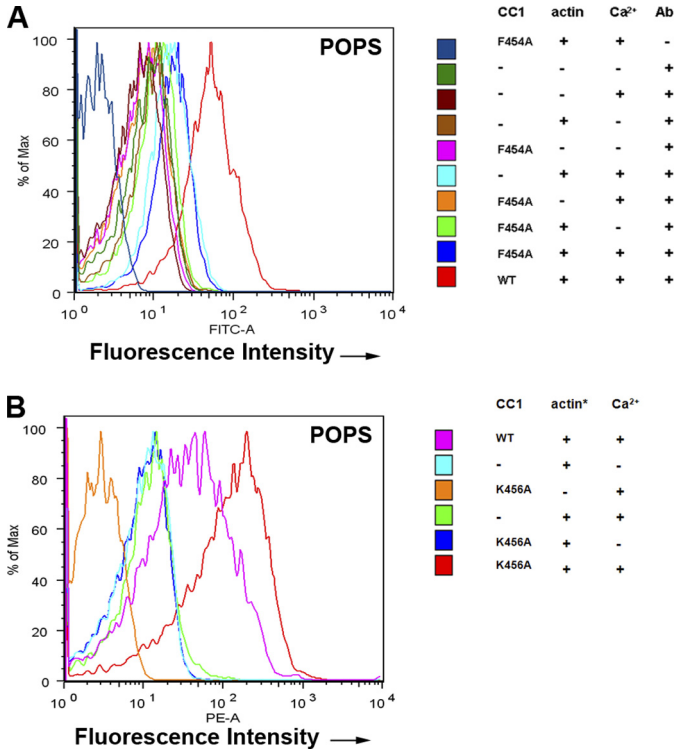


FIGURE 4. **G-actin does not bind F454A mutant and binds more strongly to K456A mutant of CEACAM1-S.** *A*, same experiment as in Fig. 3*A* except F454A mutated peptide was used. *B*, Same experiment as in *A* except K456A mutated peptide was used.

ing conformations. Each initial conformation was simulated for 100 ns with and without the addition of 2 $Ca^{2+}$ ions (simulation box size, $7 \times 7 \times 10$ nm). During all five of the MD simulations with $Ca^{2+}$ we observed a migration of $Ca^{2+}$ ions to the POPS lipid head groups, where they may mediate the interaction between CEACAM1-S and actin. K-Means clustering of the CEACAM1-S conformation over all MD trajectories revealed two distinct conformational clusters (supplemental Fig. S1). The conformations in the distinct clusters differ in the orientation of the cytoplasmic domain from Phe-454 onward with respect to the transmembrane domain (supplemental Fig. S1). The structure of the cytoplasmic and transmembrane domains by themselves is invariant between the clusters, thus suggesting that Phe-454 and its surrounding residues may serve as a hinge around which a conformational change occurs. The two different clusters exhibit differences in the orientation of Phe-454 (Fig. 5, *A–C*). In one conformation Phe-454 is pointing outward into the solvent, whereas in the other conformation Phe-454 is parallel to the lipid bilayer and buried by the surrounding lipid molecules. In the conformations where Phe-454 is buried by the surrounding lipids we observed a cation-$\pi$ interaction (25) between Phe-454 and Lys-456 (Fig. 6). This interaction is especially favored when Phe-454 is buried in the lipid bilayer. In the solvent-exposed conformations the dehydration of the amine ion of Lys-456 causes the cation-$\pi$ interaction to be unfavorable and hence broken (26). The observed cation-$\pi$ interaction between Phe-454 and Lys-456 may be one of the mechanisms by which Lys-456 inhibits actin binding. As expected, the mutation K456A relieves this inhibition (Fig. 4*B*). Simulations were also performed for the F454A mutant embedded in the lipid bilayer. The peptide conformations from these simulations clustered into a single conformation resembling the conformation of Phe-454 that points into solvent (supplemental Fig. S2). This shows that Phe-454 is required for CEACAM1-S to exist in two different conformations.

Individual simulations show no transitions from one conformational cluster to the other cluster (supplemental Fig. S1), and therefore it is speculative to discern whether addition of $Ca^{2+}$ causes one cluster to be favored over the other. NMR TROSY experiments were conducted to assess which of the two conformations is favored for actin binding and whether $Ca^{2+}$ ions have an effect on the balance between the two conformations.

*NMR Analysis of Peptide-Liposomes*—The conformation of Phe-454 in a POPS liposome environment was assessed directly by synthesis of the *N*-acyl-MUA peptide with $^{13}$C-labeled Phe and analysis by NMR TROSY. This approach allowed a clean separation of the aromatic signals of Phe-454 from the abundant phospholipid signals and had sufficient sensitivity to allow quantitation of peak volumes despite the peak broadening due to insertion of the peptide in liposomes. Two different environments (further supported in supplemental Fig. S3) were observed for Phe-454. Each environment has a distinct set of two cross-peaks (Fig. 5, *D–F*). Although three expected peaks were observed from free peptide in the absence of liposome (data not shown), it is clear that the lipid environment perturbs the pattern of cross-peaks, increasing the signal line width significantly, reducing the number of cross-peaks from three to two (for possible explanations, see supplemental NMR Discussion). The addition of actin caused a decrease in the overall intensity of the peaks as well as a change in the ratio between the peaks (Fig. 5*E* and Table 1). The decrease in peak intensity can be interpreted as binding of actin to one of the conformers which, due to an increase in molecular size, causes increased line broadening so that the signal becomes NMR invisible, the so-called "dark" state (27). The shift in ratio between the two conformations could indicate that one conformation is preferred by actin. When $Ca^{2+}$ is added, the total peak intensities are further decreased by 44% (Fig. 5*F* and Table 1), and the shift in ratios is increased, emphasizing a role for $Ca^{2+}$ in enhancing the binding of CEACAM1-S to actin.

The results of the NMR TROSY study not only support our hypothesis that the phospholipid and $Ca^{2+}$ affect the interaction of the CEACAM1-S peptide with actin, but they also suggest that two major conformers of Phe-454 exist in this environment, supporting the findings from the MD simulation study. Further NMR TROSY experiments were conducted to determine the effect of different phospholipids in the liposomes on the Phe-454 interaction with actin in the presence or absence of $Ca^{2+}$ (supplemental Figs. S3 and S4). In the POPC liposome environment, three conformers were observed, and although some peak intensities decreased with the addition of actin, there was no significant change in total peak volume upon the addition of $Ca^{2+}$ (if anything, it decreased the interaction). This result agrees with the prediction that POPC does not favor the peptide-actin interaction in the presence of $Ca^{2+}$. In the mixed POPC/POPS liposome environment, the results are essentially between the pure POPS and pure POPC environment (supplemental Table S1). The total peak volume is

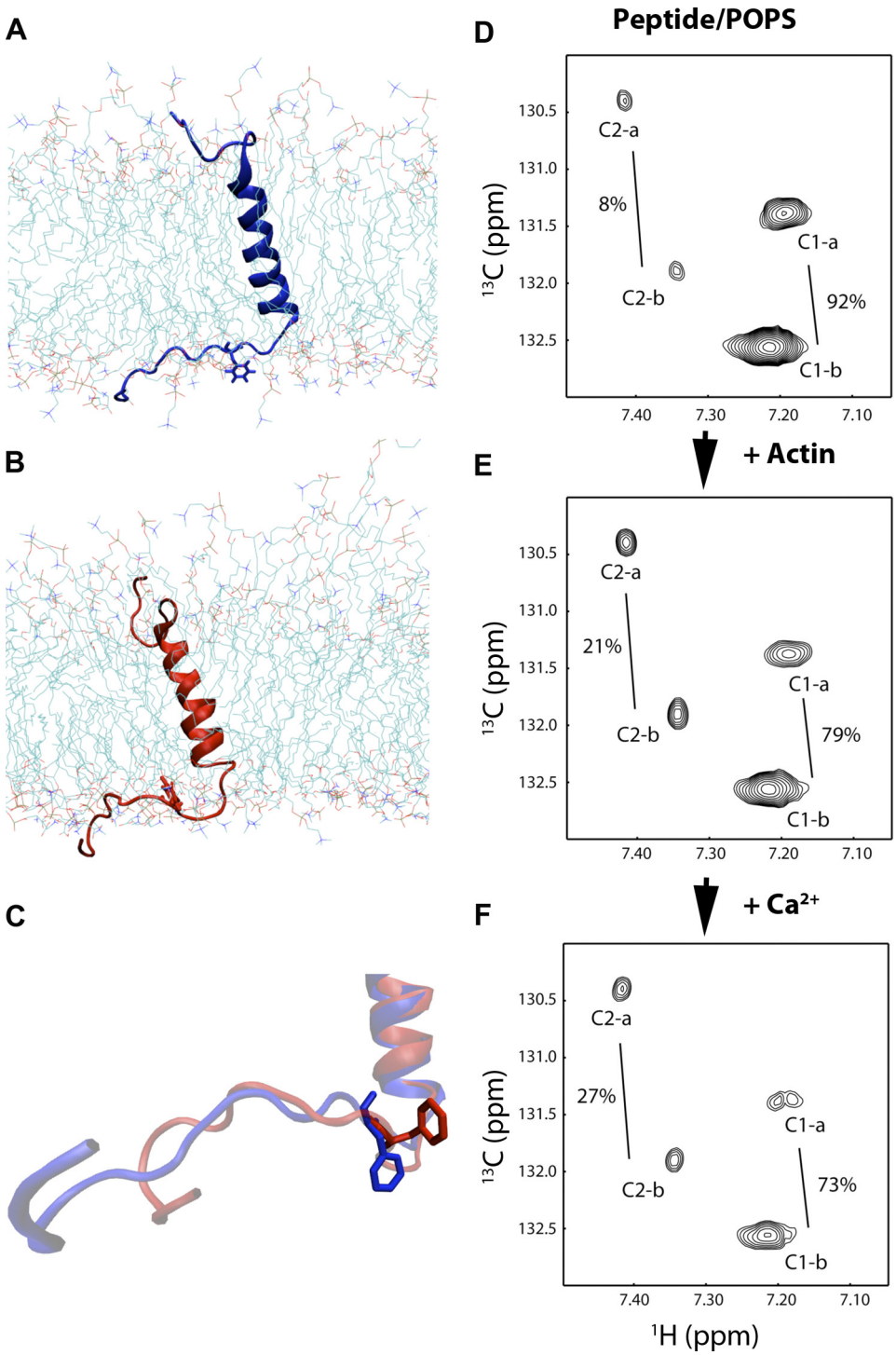


FIGURE 5. **Two major conformer ensembles predicted by MD on the CEACAM1-S peptide in an asymmetric POPS/POPC lipid bilayer and two conformations of Phe-454 in CEACAM1-S peptide inserted into POPS liposomes in the presence of actin and $Ca^{2+}$ observed by NMR.** *A–C*, MD simulations reveal two conformations that represent different environments for Phe-454. *A*, in one conformational ensemble Phe-454 is exposed to solvent surrounding the lipid bilayer. *B*, the other ensemble has Phe-454 buried in the surrounding lipid head groups. *C*, representative (nearest to mean) conformations are shown for both ensembles aligned and with Phe-454 in a *stick* representation. *D–F*, $^{13}C$-labeled Phe-454 *N*-acyl-MUA-peptide (0.1 mM) in POPS (18 mM) liposomes gives two sets of cross-peaks, C1-a and C1-b, corresponding to conformation 1, and C2-a and C2-b corresponding to conformation 2 (total percentages of each conformation indicated) as analyzed by two-dimensional NMR TROSY (*D*). The total percent of conformation 2 increases with the addition of actin (*E*) and $Ca^{2+}$ (*F*).

decreased by 15% upon the addition of $Ca^{2+}$ to the complex of actin and peptide.

To address whether $Ca^{2+}$ affects the interaction between G-actin and CEACAM1-S peptide by perturbation of the equilibrium between two conformations of Phe-454, we carried out an NMR experiment on free peptide in the POPS environment with different concentrations of $Ca^{2+}$ in the absence of actin. We found that [$Ca^{2+}$] *per se* does not affect the equilibrium

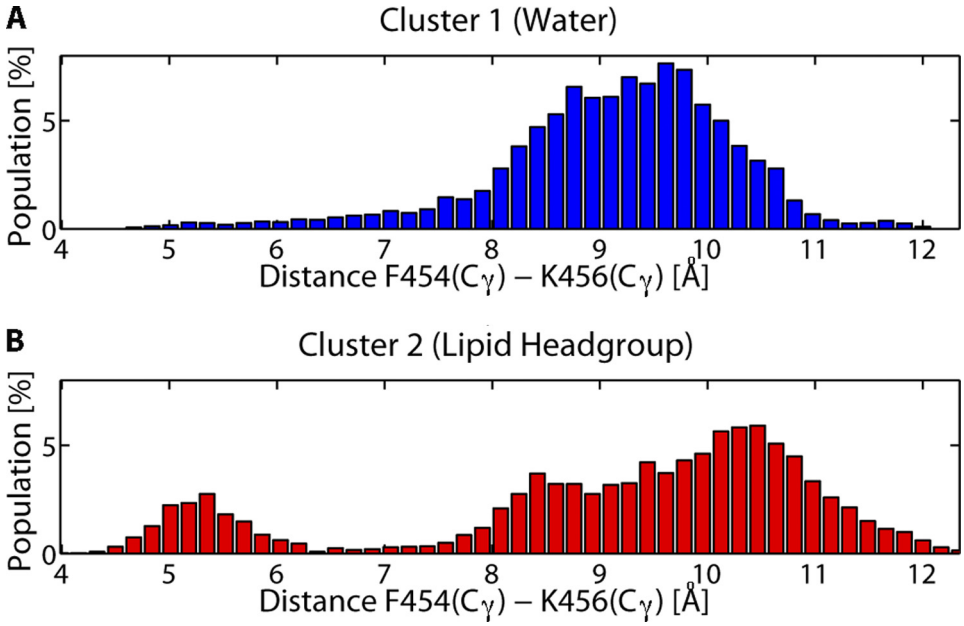


FIGURE 6. **Cation-$\pi$ interaction observed between Phe-454 and Lys-456 only when Phe-454 is in the lipid head groups.** The distributions of $C_\gamma$–$C_\gamma$ distances between Phe-454 and Lys-456 sampled during MD are shown. *A*, when Phe-454 is solvent-exposed (*blue* conformation) there is only one peak in the distribution observed at ~9.5 Å, indicating that there is no interaction between Phe-454 and Lys-456. *B*, when Phe-454 is in the lipid head groups (*red* conformation) an additional peak in the distribution is observed at ~5.2 Å, indicating an interaction between Phe-454 and Lys-456.

**TABLE 1**

**NMR peak volumes of $^{13}$C-Phe-CEACAM1-S peptide in POPS liposome**

All peak volumes are corrected against factors of number of scans and the dilution due to addition of $Ca^{2+}$ to the system.

| Peak[a] | $V_{pep}$[b] | $V_{pep\_act}$[c] | $(V_{pep\_act} - V_{pep})/V_{pep}$ | $V_{pep\_act\_Ca^{2+}}$[d] | $(V_{pep\_act\_Ca^{2+}} - V_{pep})/V_{pep}$ |
|---|---|---|---|---|---|
| C1-a | 1,006 | 684 | −32% | 396 | −61% |
| C1-b | 2,408 | 1,732 | −28% | 857 | −64% |
| C2-a | 147 | 301 | 105% | 236 | 61% |
| C2-b | 153 | 326 | 113% | 223 | 46% |
| Total | 3,714 | 3,043 | −18% | 1,712 | −54% |

[a] Peak symbols (C1-a/b and C2-a/b) are shown in Fig. 5.
[b] $V_{pep}$ is the peak volume measured from the free CEACAM1-S peptide in the liposome.
[c] $V_{pep\_act}$ is the peak volume measured from the complex of CEACAM1-S and actin.
[d] $V_{pep\_act\_Ca^{2+}}$ is the peak volume measured from the complex of CEACAM1-S and actin in the presence of 5 mM $Ca^{2+}$.

between the two conformers (supplemental Fig. S5 and supplemental Table S2). Thus, most likely, $Ca^{2+}$ is first recruited to the negatively charged phospholipid, which in turn, enhances the peptide-G-actin interaction. In other work, although G-actin has been shown to interact directly with negatively charged liposomes (28), the additional effect of inserted peptides has not been studied.

The NMR analysis also indicates that pH affects the equilibrium of the two observed conformations of the peptide embedded in the lipid (supplemental Fig. S3, *A* and *B*). Because $Ca^{2+}$ is a better studied signal transducer at the plasma membrane compared with pH, the effects of pH were not studied further.

*Analysis by Surface Plasmon Resonance*—A third approach to assess the peptide-G-actin interaction in a phospholipid environment is the use of surface plasmon resonance where a phospholipid bilayer can be monolayered onto a hydrophobic chip (29). In this approach, a lipid monolayer of POPS was applied to an existing hydrophobic substrate, *N*-acyl-MUA-peptide was inserted into the upper phospholipid layer, and the subsequent binding of actin was monitored in the presence or absence of $Ca^{2+}$. The results demonstrate that *N*-acyl-MUA peptide binds in a saturable manner to the POPS phospholipid monolayer and that actin binding requires $Ca^{2+}$ (supplemental Fig. S6).

## DISCUSSION

Three completely different experimental approaches, together with MD simulations, demonstrate a requirement for negatively charged phospholipid POPS and $Ca^{2+}$ in the regulation of the binding of G-actin to the cytoplasmic domain peptide of CEACAM1-S. In the first approach, POPS or POPC liposomes mimicking the inner or outer leaflet of the plasma membrane, respectively, were coated onto 4.5-$\mu$m glass beads, *N*-acyl-MUA-peptide was inserted into the outer leaflet, and the binding of actin was monitored in the presence or absence of $Ca^{2+}$. This approach has the advantage that it creates a cell-sized lipid surface that allows specification of interacting components present at either the inside or outside of the cell membrane and measurement of interactions by flow cytometry using fluorescent labeling of components of interest. This approach validated our earlier finding that Phe-454 plays an essential role in actin binding (5). A disadvantage of the approach is that it provides no direct evidence of the molecular state of the inserted peptide. To assess this information, we

performed NMR analysis on the $^{13}C$-labeled peptide (at the residue of interest) inserted into liposomes under a variety of conditions. This approach demonstrated that $Ca^{2+}$ played a major role in the peptide-actin interaction and not in the peptide-phospholipid interaction. An advantage of this approach is the use of liposomes that more accurately reflect the lipid environment in the cell as opposed to the conventional use of peptides embedded in micelles.

In our model system 1 mM $Ca^{2+}$ was required to effect actin binding. Although the global concentration of $Ca^{2+}$ in the cytoplasm during signaling peaks at about 1.4 $\mu$M, the local concentration of $Ca^{2+}$ in the microenvironment around the cytoplasm adjacent to the cell membrane would be in the millimolar range due to the effect of calcium ion channel proteins and/or calcium transporters that produce a spike in the local $Ca^{2+}$ concentration. Because our liposomes lack the presence of these $Ca^{2+}$ transporters, a millimolar bulk concentration of $Ca^{2+}$ was used to mimic the local environment in the cell. The difference between local and global concentrations of $Ca^{2+}$ can be visualized in our molecular simulations shown in Fig. 5, *A–C*, where we have added only two $Ca^{2+}$ ions to the lipid bilayer-cytosol box ($7 \times 7 \times 10$ nm). This leads to a local $Ca^{2+}$ concentration of about 8 mM. If we simulated the physiological global concentration of $Ca^{2+}$ inside activated cells we would either have to use a box $10^3$ times larger or assume $10^{-3}$ $Ca^{2+}$ ions in our box, assumptions that are illogical. We believe that these considerations justify our use of 1 mM $Ca^{2+}$ in our experiments.

A potential disadvantage of the NMR method is that the overall molecular size (including the lipid bilayer) of the system is quite large, and thus a millimolar sample concentration is needed to compensate for the increased line width of NMR peaks. Thus, we employed a third approach, namely the use of surface plasmon resonance that has the advantage of allowing kinetic measurements of the binding of various components to each other at lower concentrations. This method also confirmed $Ca^{2+}$ and lipid specific requirements for G-actin binding to lipid-embedded CEACAM1-S peptide. However, this method suffers from the lack of structural information. Thus, we performed MD simulations to gain access to changes in the entire peptide embedded in the lipid bilayer at the atomic level. This approach allowed us to provide a theoretical basis for our findings and to make predictions that could be validated by further experiments. A combination of MD simulations and NMR experiments reveal two reversible conformational states of Phe-454. The population of these states is not affected by varying the $Ca^{2+}$ concentration but does change on actin binding. MD simulations predict that in one conformation Phe-454 is solvent-exposed whereas in the other conformation Phe-454 is buried in the lipid head groups. Furthermore, MD simulations show that the conformation with Phe-454 buried in the lipid head groups may be stabilized by a cation-$\pi$ interaction (25, 30) of Lys-456 with Phe-454. This predicted cation-$\pi$ interaction, and its role in conformational selection, could explain why mutation of Lys-456 affects actin binding in a positive manner. Finally, we performed MD simulations for the F454A mutant peptide and found that Ala-454 was unable to adopt two confirmations in the lipid bilayer, strengthening our use of MD as a method to examine the structural constraints of the model system.

Our findings help explain why many receptor cytoplasmic domain peptides, especially those as short as the CEACAM1-S peptide, may have highly specific and tunable interactions with components of the cytosol. Previously, receptor aggregation was proposed as a major mechanism for activation of cytoplasmic domains in downstream signaling (31, 32). However, this mechanism is inadequate to account for the cooperative effect of the local phospholipid environment and $Ca^{2+}$ signaling. In terms of the downstream interacting protein G-actin, it has been shown previously that it is attracted to negatively charged phospholipids (28), but this interaction alone is insufficient to confer membrane site specificity or temporal control by $Ca^{2+}$ signals. Indeed, for actin to polymerize at the right location and time at the membrane, it must find a suitable binding partner that responds to rapid signals from both the outside (say receptor clustering) and inside (say $Ca^{2+}$ signaling). CEACAM1-S provides the outside activation step by receptor clustering during its cell-cell interactions (31) and the inside activation step via $Ca^{2+}$-generated interactions at Phe-454 in the negatively charged phospholipid environment. In the case of CEACAM1-S, the source of the intracellular $Ca^{2+}$ is likely from other receptors that become activated during cell-cell interactions, including G protein-coupled receptors (33, 34). In this respect, both CEACAM1 (35–37) and G protein-coupled receptors (38) reside within the same lipid microenvironments, emphasizing their local ability to coordinate signals. Finally, for actin to polymerize, it must be correctly oriented to form the characteristic double helix of F-actin. In the case of CEACAM1-S, the polymerization would occur directly adjacent to the phospholipid bilayer, exactly the situation seen for the formation of cortical actin. Thus, it is likely that cortical actin formation is dynamic, responding to cell-cell interactions that allow local changes in the distribution of receptors at the cell surface (for an example of the redistribution of CEACAM1-S and actin during cell-cell adhesion, see Fig. 1).

In summary, these findings explain how receptors with short cytoplasmic tails can recruit cytosolic proteins in a phospholipid- and calcium-specific manner. In addition, these models provide a powerful approach that can be applied to other membrane protein interactions.

*Acknowledgment—Preliminary flow studies were performed by Keith Le.*

## REFERENCES

1. Brozinick, J. T., Jr., Berkemeier, B. A., and Elmendorf, J. S. (2007) *Curr. Diabetes Rev.* **3,** 111–122
2. Scita, G., Confalonieri, S., Lappalainen, P., and Suetsugu, S. (2008) *Trends Cell Biol.* **18,** 52–60
3. Weed, S. A., and Parsons, J. T. (2001) *Oncogene* **20,** 6418–6434
4. Huang, Y., and Burkhardt, J. K. (2007) *J. Cell Sci.* **120,** 723–730
5. Chen, C. J., Kirshner, J., Sherman, M. A., Hu, W., Nguyen, T., and Shively, J. E. (2007) *J. Biol. Chem.* **282,** 5749–5760
6. Ko, K. S., Arora, P. D., Bhide, V., Chen, A., and McCulloch, C. A. (2001) *J. Cell Sci.* **114,** 1155–1167
7. Clapham, D. E. (2007) *Cell* **131,** 1047–1058
8. Kandt, C., Ash, W. L., and Tieleman, D. P. (2007) *Methods* **41,** 475–488

9. Tieleman, D. P., Forrest, L. R., Sansom, M. S., and Berendsen, H. J. (1998) *Biochemistry* **37,** 17554–17561
10. Berendsen, H. J., Postma, J. P., van Gunsteren, W. F., and Hermans, J. (1981) in *Intermolecular Forces*, (Pullman, B., ed) pp. 331–342. Reidel, Dordrecht, The Netherlands
11. Van Der Spoel, D., Lindahl, E., Hess, B., Groenhof, G., Mark, A. E., and Berendsen, H. J. (2005) *J. Comput. Chem.* **26,** 1701–1718
12. Oostenbrink, C., Villa, A., Mark, A. E., and van Gunsteren, W. F. (2004) *J. Comput. Chem.* **25,** 1656–1676
13. Berger, O., Edholm, O., and Jähnig, F. (1997) *Biophys. J.* **72,** 2002–2013
14. Essmann, U., Perera, L., Berkowitz, M. L., Darden, T., Lee, H., and Pedersen, L. G. (1995) *J. Chem. Phys.* **103,** 8577–8593
15. Hess, B., Bekker, H., Berendsen, H. J., and Fraaije, J. G. (1997) *J. Comput. Chem.* **18,** 1463–1472
16. Bussi, G., Donadio, D., and Parrinello, M. (2007) *J. Chem. Phys.* **126,** 014101
17. Parrinello, M., and Rahman, A. (1981) *J. Appl. Phys.* **52,** 7182–7190
18. Nosé, S., and Klein, M. L. (1983) *Mol. Phys.* **50,** 1055–1076
19. Nose, S. (1984) *J. Chem. Phys.* **81,** 511–519
20. Wider, G., and Dreier, L. (2006) *J. Am. Chem. Soc.* **128,** 2571–2576
21. Vuister, G. W., and Bax, A. (1992) *J. Magn. Reson.* **98,** 428–435
22. Pervushin, K., Riek, R., Wider, G., and Wuthrich, K. (1998) *J. Am. Chem. Soc.* **120,** 6394–6400
23. Delaglio, F., Grzesiek, S., Vuister, G. W., Zhu, G., Pfeifer, J., and Bax, A. (1995) *J. Biomol. NMR* **6,** 277–293
24. Johnson, B. A., and Blevins, R. A. (1994) *J. Biomol. NMR* **4,** 603–614
25. Dougherty, D. A. (1996) *Science* **271,** 163–168
26. Kumpf, R. A., and Dougherty, D. A. (1993) *Science* **261,** 1708–1710
27. Fawzi, N. L., Ying, J., Torchia, D. A., and Clore, G. M. (2010) *J. Am. Chem. Soc.* **132,** 9948–9951
28. Bouchard, M., Pare, C., Dutasta, J. P., Chauvet, J. P., Gicquaud, C., and Auger, M. (1998) *Biochemistry* **37,** 3149–3155
29. Ida, M., Satoh, A., Matsumoto, I., and Kojima-Aikawa, K. (2004) *J. Biochem.* **135,** 583–588
30. Dougherty, D. A. (2007) *J. Nutr.* **137,** 1504S–1508S; discussion 1516S–1517S
31. Gray-Owen, S. D., and Blumberg, R. S. (2006) *Nat. Rev. Immunol.* **6,** 433–446
32. Müller, M. M., Klaile, E., Vorontsova, O., Singer, B. B., and Obrink, B. (2009) *J. Cell Biol.* **187,** 569–581
33. Werry, T. D., Wilkinson, G. F., and Willars, G. B. (2003) *Biochem. J.* **374,** 281–296
34. Bouschet, T., Martin, S., and Henley, J. M. (2008) *Trends Pharmacol. Sci.* **29,** 633–639
35. Thorp, E. B., and Gallagher, T. M. (2004) *J. Virol.* **78,** 2682–2692
36. Chen, C. J., and Shively, J. E. (2004) *J. Immunol.* **172,** 3544–3552
37. Muenzner, P., Bachmann, V., Kuespert, K., and Hauck, C. R. (2008) *Cell Microbiol.* **10,** 1074–1092
38. Fallahi-Sichani, M., and Linderman, J. J. (2009) *PLoS One* **4,** e6604